



Development of core–shell structured nanoparticle for sequential release of tariquidar and docetaxel to overcome multi drug-resistant cancer

Hyun Min Jung¹ · Chang Hyun Kim^{1,2} · Jo-Eun Seo¹ · Yoon Tae Goo¹ · Sun Ho Hong¹ · Myung Joo Kang³ · Sangkil Lee¹ · Young Wook Choi¹

Received: 26 July 2023 / Accepted: 30 October 2023 / Published online: 29 November 2023
© The Author(s) under exclusive licence to The Korean Society of Pharmaceutical Sciences and Technology 2023

Abstract

Purpose We developed a core–shell (CS) nanoparticle, docetaxel (DTX)-loaded core and tariquidar (TRQ)-loaded shell conjugated with PEG and RIPL peptide (D/C-T/S-PR), which sequentially releases TRQ and DTX to overcome multidrug resistant (MDR) cancer.

Methods D/C-T/S-PR was fabricated by two-step method, including the formation of a DTX-loaded nanostructured lipid carrier (D/NLC) core by solvent emulsification–evaporation and a TRQ-loaded lipid bilayer shell using a film hydration method. CSs with a lipid mass ratio of shell to core from 1 to 5 (CS1–CS5) were prepared and purified by sucrose density gradient centrifugation. The physicochemical properties of the CSs were evaluated to select an optimal ratio. Additionally, CS formation was confirmed by transmission microscopy (TEM) and confocal laser scanning microscope (CLSM) images. In vitro drug release was evaluated and in vitro cellular uptake and cytotoxicity were assessed against MCF7 and MCF7/ADR cells.

Results The amounts of CSs acquired after purification were increased with increasing lipid ratio. CS3 was selected as the final formulation due to its high drug loading. Using TEM, we observed the distinct formation of the shell coating the core in the D/C-T/S-PR, while CLSM was used to confirm the co-loading of two fluorescent probes in different layers. D/C-T/S-PR showed a burst release of TRQ from the shell, followed by sustained release of DTX from the core. D/C-T/S-PR showed enhanced uptake and cytotoxicity in both cell types.

Conclusion We successfully developed a CS exhibiting sequential release of TRQ and DTX, which may represent a promising strategy to overcome MDR.

Keywords Core–shell · Sequential release · Tariquidar · Docetaxel · Multidrug resistance

Introduction

Docetaxel (DTX) belongs to the second-generation taxane family and is an anticancer agent used to treat breast, ovarian, prostate, and non-small-cell lung cancers (Yin et al. 2009; Patel et al. 2015). DTX has an affinity to β -tubulin and is a mitotic inhibitor that induces tubulin polymerization and mitotic arrest in the cell cycle at the G2/M phase (Xu et al. 2016; Li et al. 2021). However, the poor aqueous solubility, nonspecific toxicity, and especially multidrug resistance (MDR) of DTX can limit its clinical

application despite its increased usage (Guo et al. 2017). The overexpression of P-glycoprotein (P-gp), as a drug-efflux transporter, is the main reason for MDR, and anticancer agents that are responsive to P-gp, including DTX, doxorubicin, and vinblastine, can be pumped out from the cell membrane to reverse concentration gradients, leading to a reduced intracellular concentration in tumor cells (Sarisozen et al. 2012; Zhong et al. 2020).

Combination therapy with P-gp inhibitors and DTX has been widely studied to improve therapeutic efficacy against MDR (Patil et al. 2009). Tariquidar (TRQ) is a third-generation P-gp inhibitor, which is more potent and specific to P-gp and has lower toxicity, better tolerability, and fewer pharmacokinetic interactions with anticancer drugs compared to first- and second-generation P-gp inhibitors (Thomas and Coley 2003; Patil et al. 2009). The

Hyun Min Jung and Chang Hyun Kim have contributed equally to this work.

Extended author information available on the last page of the article

mechanism by which TRQ acts on tumor cells is via non-competitive binding to P-gp, which inhibits its drug-binding conformation and prevents substrate binding (Xia et al. 2018; Zhong et al. 2020). Although TRQ can increase the therapeutic efficacy of MDR cancer, it has poor aqueous solubility, a nonspecific distribution, and side effects on normal cells (Xia et al. 2018). To overcome these disadvantages and increase the efficacy of anticancer agents, drugs should be co-delivered into the same target using a precise nanocarrier system (Patil et al. 2009).

Nanoparticles can offer diverse possibilities for addressing complex and challenging chemotherapy by providing a broad spectrum of treatment opportunities (Thapa and Kim 2023). When considering the mechanism of P-gp, a nanoparticle-based drug delivery system that provides sequential release of P-gp inhibitors and anticancer agents is essential for MDR treatment (Zhang et al. 2017). The rapid release of P-gp inhibitors can suppress the action of P-gp efficiently, while the inclusion of an anticancer agent can maintain sustained release (Zhang et al. 2017). Additionally, when considering the drug–drug interaction associated with P-gp, sequential release can avoid or minimize interactions with drugs and has limited side effects by loading the drugs in different spaces and enhancing target specificity (Yap et al. 2013; Lee et al. 2023). A core-shell (CS) can be an appropriate model to release drugs sequentially given that the concentration of the first released drug can reach the required level rapidly, while that of the second released drug can be maintained at a steady level (Sengupta et al. 2005).

The structure of a CS involves a core surrounded by a shell, which can be used to encapsulate and deliver two or more therapeutic agents into each compartment (Mandal et al. 2013). Indeed, lipid-coated CSs have been widely used in recent years due to their biocompatibility, stability, high specificity by surface modification, sustained release of the core, and ability to co-load drugs into each space (Jiang et al. 2020). For example, Zhang et al. (2017) fabricated a CS to co-load paclitaxel and tetrandrine with a sequential drug-release profile, while Ruttala and Ko (2015) co-delivered curcumin and paclitaxel using a CS and showed a sequential release pattern that enhanced chemotherapeutic efficacy. General CS-structured drug delivery systems introduced the simple co-loading of two types of anti-cancer drugs into the core and shell layers. In addition, most studies have mainly introduced application of two different types of anticancer drugs together to improve anticancer effects.

However, in the present study, we propose a new strategy for chemotherapy in that DTX is loaded in the core, TRQ, a P-gp inhibitor, was loaded in the shell, and IPLVVPLRRR RRRRRRRC (RIPL) peptide that composed of two domains, RRRRRRRRRC (R8) a cell penetrating peptide domain and

IPLVVPLC (IPL) hepsin-specific sequences domain, to improve targeting ability to cancer cells by enhanced cellular uptake. The RIPL peptide was firstly proposed as a cell penetrating/homing peptide in previous report (Kang et al. 2014) and applied to this work for the same purposes. Based on the previous work, we developed a CS nanoparticle, encompassing a DTX-loaded core and TRQ-loaded shell conjugated with polyethylene glycol (PEG) and RIPL peptide (D/C-T/S-PR), to provide sequential release of TRQ and DTX. D/C-T/S-PR was prepared by a two-step method, including the formation of a DTX-loaded nanostructured lipid carrier (D/NLC) core by solvent-evaporation emulsification and a TRQ-loaded lipid bilayer shell using a film hydration method (Fig. 1). CSs with a lipid mass ratio of shell to core from 1 to 5 (CS1–CS5) and a 1:1 mass ratio of DTX and TRQ were prepared and purified. After purification, the physicochemical properties of the CSs, including the particle size, polydispersity index (PDI), zeta potential (ZP), encapsulation efficiency (EE), and drug loading (DL) were evaluated to select an optimal lipid ratio and for physical stability. Also, morphology was evaluated to confirm the CS formation. Moreover, the *in vitro* drug release patterns were evaluated for 48 h, while the *in vitro* antitumor efficacy was assessed in terms of cellular uptake and cytotoxicity against MCF7 and MCF7/ADR cells.

Materials and methods

Materials

DTX (purity > 99%) was received from Chong Kun Dang Pharm. Co. (Yongin, Korea); TRQ (purity > 97.5%) was purchased from MedChemExpress (Monmouth Junction, NJ, USA); oleoyl macrogol-6 glycerides (Labrafil® M 1944 CS) and glyceryl distearate (Precirol® ATO 5) were received from Gattefosse (Saint-Priest, France); dioctadecyl-3,3,3',3'-tetramethylindocarbocyanine perchlorate (DiI), coumarin 6 (C6), dichloromethane (DCM), polyvinyl alcohol (PVA), polysorbate 20 (Tween® 20), dimethyl sulfoxide (DMSO), phosphotungstic acid, sodium dodecyl sulfate (SDS), and phosphate buffer saline (PBS) tablets were purchased from Sigma-Aldrich Co. (St. Louis, MO, USA); L- α -phosphatidylcholine (Soy PC), 1,2-distearoyl-sn-glycero-3-phosphoethanolamine-N-[maleimide (polyethylene glycol)-2000] (DSPE-PEG2K-Mal), and 1,2-distearoyl-sn-glycero-3-phosphoethanolamine-N-[methoxy(polyethylene glycol)-3000] (DSPE-PEG3K) were purchased from Avanti Polar Lipids (Alabaster, AL, USA); and RIPL peptide was synthesized by Pepton Co. (Daejeon, Korea).

For cell experiments, human breast adenocarcinoma (MCF7) cells were purchased from the Korean Cell Line Bank (Seoul, Korea), while MDR human breast

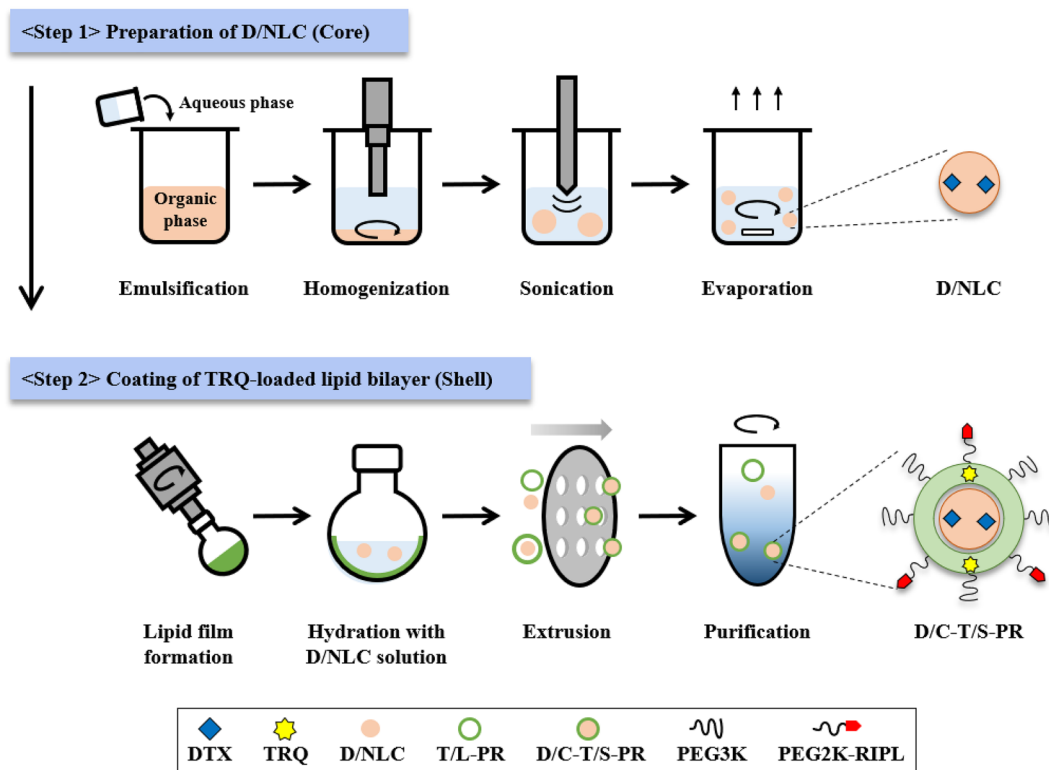


Fig. 1 Schematic illustration of core-shell formation process. First, preparation of docetaxel-loaded nanostructured lipid carrier (D/NLC) core. Second, coating of tariquidar (TRQ)-loaded lipid bilayer shell. Briefly, D/NLC core was prepared by solvent emulsification-evapora-

tion. Then, lipid film was hydrated with the D/NLC core solution, and the resulting suspension was extruded and subjected to the sucrose density gradient centrifugation (SDGC) to purify the core-shell

adenocarcinoma (MCF7/ADR) cells were kindly donated by Prof. Dr. Kyung Hoon Min (College of Pharmacy, Chung-Ang University, Seoul, Korea). Cell culture materials, including Roswell Park Memorial Institute (RPMI) 1640 medium, fetal bovine serum (FBS), penicillin–streptomycin, and trypsin–EDTA (0.25%), were obtained from Invitrogen (Carlsbad, CA, USA). EZ-cytox water-soluble tetrazolium salt-1 (WST-1) reagent solution was purchased from Dali Lab service (Seoul, Korea), and 4',6-diamidino-2-phenylindole (DAPI) was purchased from Vector Laboratories (Burlingame, CA, USA).

Synthesis of DSPE-PEG2K-RIPL

DSPE-PEG2K-RIPL was synthesized by a thiol-maleimide reaction with DSPE-PEG2K-Mal and RIPL peptide based on a previous report (Kim et al. 2023). In brief the maleimide group of DSPE-PEG2K-Mal was reacted with the sulfhydryl group of the cysteine residue of the RIPL peptide to obtain a thioether bond. Briefly, DSPE-PEG2K-Mal was mixed with RIPL peptide at a molar ratio of 1:1.12 in 0.01 M PBS (pH 7.4) for 48 h at 25 °C in the dark. Then, unreacted RIPL peptides were removed by purification using a

3.5-kDa dialysis membrane for 24 h at 4 °C. After dialysis, the purified solution was freeze-dried for 24 h at –45 °C using a freeze-dryer (FDU-1200; EYELA, Miyagi, Japan) at a pressure of 8 Pa, and the dried sample was stored at 4 °C for subsequent experiments.

Preparation of reference solutions

DTX-containing solution (D-Sol) was prepared as a commercial product called Taxotere® (Guo et al. 2017). Briefly, DTX was mixed with double-distilled water containing Tween 80 (25%, w/v) and ethanol (9.75%, w/v). TRQ-containing solution (T-Sol) was prepared by dissolving TRQ in DMSO. The final concentration of DTX in D-Sol and TRQ in T-Sol was 10 mg/mL and 5 mg/mL, respectively. For in vitro cell experiments, D-Sol and T-Sol were diluted with cell culture media and the final concentration of DMSO was <0.1%.

Preparation of nanoparticle formulations

According to the solvent emulsification-evaporation method reported previously (Kim et al. 2023), NLC formulations

were prepared in the following groups: Empty NLC, D/NLC, and DTX- and TRQ-loaded NLC-PR (DT/NLC-PR). TRQ-loaded liposome-PR (T/L-PR) was prepared by the film hydration method reported previously (Jang et al. 2019). Empty core-shell-PR (CS-PR), DTX-loaded core and TRQ-loaded shell conjugated with PEG (D/C-T/S-P), and D/C-T/S-PR were prepared by the 2-step method reported previously, with slight modification (Wang and Ho 2010). The lipid film was hydrated with the NLC core and the resulting suspension was extruded and subjected to sucrose density gradient centrifugation (SDGC) to separate the CSs. To observe the nanoparticles after SDGC or co-loading of two fluorescent probes in the core and shell, DiI was loaded in NLC and core and C6 was loaded in the liposome and shell. All of the prepared nanoparticle samples were stored at 4 °C and used within 2 weeks.

Preparation of NLC

To prepare the D/NLC, an organic phase containing labrafil M 1944 CS (liquid oil; 6.2 µL), precirol ATO 5 (solid lipid; 15.5 mg), DiI (40 µg), and DTX (1.6 mg) was dissolved in DCM (670 µL). The organic phase was added into the aqueous phase (4 mL) containing Tween 20 (2%, w/v) and PVA (0.5%, w/v). Subsequently, the mixture was homogenized at 15,000 rpm for 2 min using an Ultra-Turrax T25 basic homogenizer (IKA Labortechnik, Staufen, Germany). The resulting suspension was sonicated using a probe-type sonicator (Sonoplus, HD2070; Bandelin Electronics, Berlin, Germany) for 3 min at 4 °C. Finally, the emulsion was evaporated at 400 rpm for 4 h using a magnetic stirrer to remove the organic solvent. DT/NLC-PR was prepared separately using the same procedure, except that DSPE-PEG3K (5 mol%) and TRQ (1.6 mg) were added into the organic phase and Tween 20 (1%, w/v) instead of Tween 20 (2%, w/v) and DSPE-PEG2K-RIPL (1 mol%) were added into the aqueous phase. The empty NLC was prepared using the same procedure, except the addition of DTX.

Preparation of liposomes

To prepare T/L-PR, soy PC:Tween 20:DSPE-PEG3K:DSPE-PEG2K-RIPL (molar ratio = 79.2:8.8:10:2), C6 (40 µg), and TRQ (1.6 mg) were dissolved in DCM in a round-bottom flask. Then, the organic phase was evaporated with a rotary vacuum evaporator at 40 rpm for 5 min to form a lipid film in the flask. Subsequently, the dried lipid film was hydrated with double-distilled water (4 mL) at a temperature higher than the transition temperature (40 °C) to allow the lipid film to form lipid bilayers spontaneously. Finally, the resulting suspension was extruded 20 times through 400-nm

polycarbonate membrane (Nuclepore™ Track-Etch Membrane, CYTIVA, Germany) with a syringe extruder to obtain a homogenous size distribution.

Preparation of CS

A schematic illustration of the CS preparation and the representative structure of D/C-T/S-PR are depicted in Fig. 1. D/NLC, as the core material, was used for the hydration of the lipid film composed of soy PC:Tween 20:DSPE-PEG3K:DSPE-PEG2K-RIPL (molar ratio = 79.2:8.8:10:2), C6 (40 g), and TRQ (1.6 mg). The same procedures as those for making T/L-PR were used during the hydration process and extrusion. Additionally, to decide the optimal lipid ratio of shell to core and ensure maximum drug loading, the CSs were manufactured from CS1 to CS5, while the mass ratio of DTX and TRQ was set to 1:1. As depicted in Fig. 2A, we conducted SDGC to acquire CSs at a specific density compartment. Briefly, to generate the sucrose density gradient, 750 µL of sucrose (8%, w/v) was added to a 1.5-mL microtube, before adding 50 µL of sucrose (50%, w/v) below by inserting the pipette to the very bottom of the microtube. Next, 200 µL of sample was loaded on the top of the 8% sucrose and centrifuged for 1 h at 20,000×g at 4 °C. Subsequently, the lower layer containing nanoparticles was sampled to select the D/C-T/S-PR according to its physicochemical properties (Fig. 2B). To wash the sucrose from the D/C-T/S-PR solution, the solution was ultracentrifuged using Amicon® ultracentrifugal filters (30 kDa molecular weight cutoff; Millipore, Billerica, MA, USA). Briefly, the D/C-T/S-PR solution was centrifuged for 2 h at 2,500 × g at 4 °C. Then, the concentrate in the filter was inverted and recentrifuged for 5 min at 2,500 × g at 4 °C, followed by resuspension with an equal volume of double-distilled water. Finally, physical stability of D/C-T/S-PR was evaluated by particle size, PDI, ZP, and EE of DTX and TRQ at 4 °C for 7 days (Fig. 2C). D/C-T/S-P was prepared separately using the same procedure with the selected optimal ratio above, except that DSPE-PEG2K-RIPL was not added. CS-PR was prepared using the same procedure with the selected optimal ratio above, except the addition of DTX and TRQ.

Particle size and ZP analysis

The average particle size, PDI, and ZP of various nanoparticles were determined using a dynamic light scattering (DLS) particle size analyzer (Zetasizer Nano-ZS; Malvern Instruments, UK). All measurements were conducted at 25 °C and each sample was measured in triplicate after 100 times dilution with double distilled water.

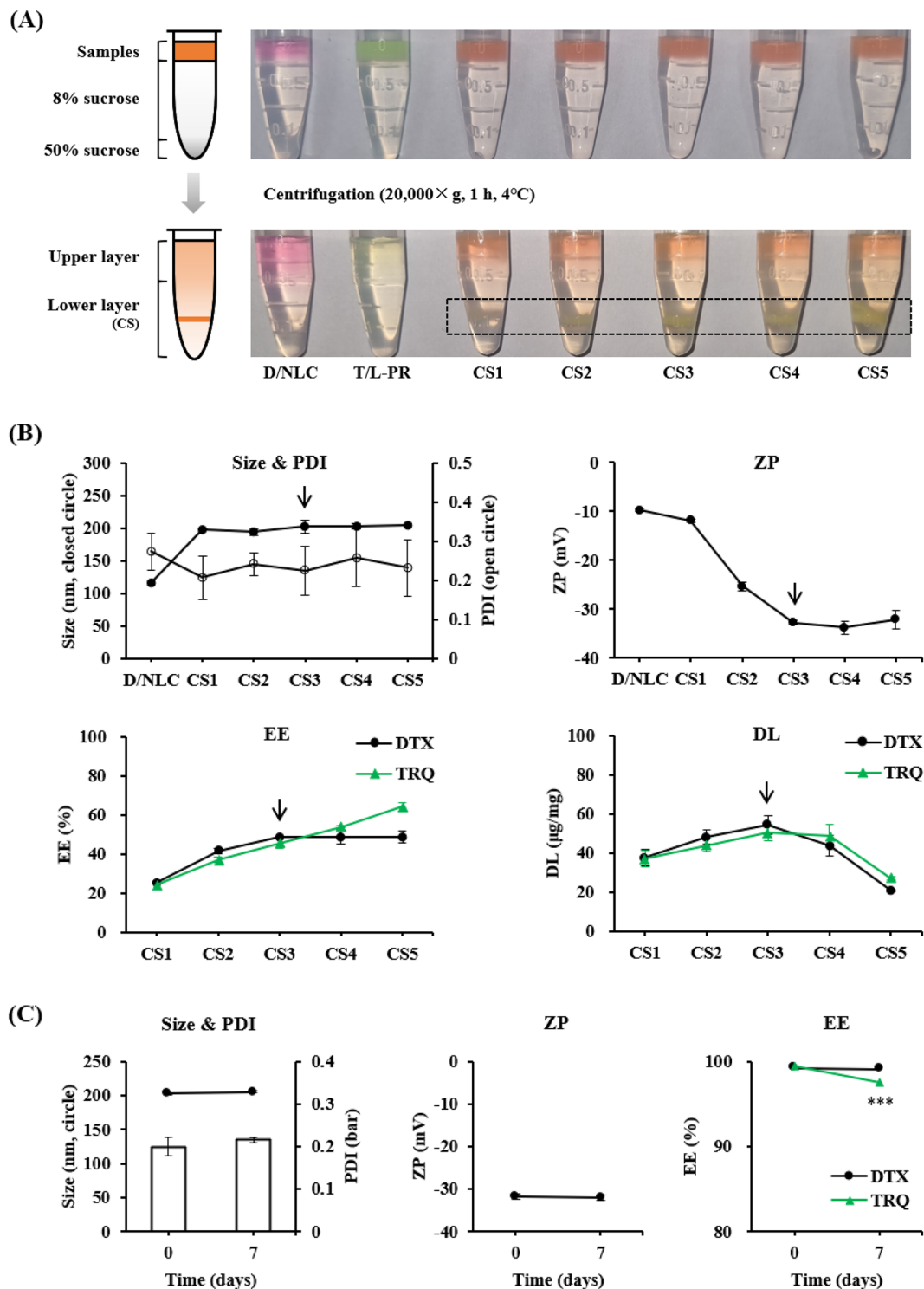


Fig. 2 Purification of the core–shell (CS) by sucrose density gradient centrifugation, determination of the optimal lipid ratio of shell to core by characterization, and physical stability of the final formulation for 7 days. CSs with a lipid mass ratio of shell to core from 1 to 5 (CS1–CS5) were prepared. **A** Samples including docetaxel (DTX)-loaded nanostructured lipid carrier (D/NLC), tariquidar (TRQ)-loaded liposome conjugated with PEG and RIPL peptide (T/L-PR), and CSs were added on top of the tube containing sucrose with a concentration gradient. Subsequently, the samples were centrifuged for 1 h

at $20,000 \times g$ at $4^\circ C$ and the lower layer was sampled to evaluate its physicochemical properties. **B** Effect of the lipid ratio of shell to core on the particle size, polydispersity index (PDI), zeta potential (ZP), encapsulation efficiency (EE), and drug loading (DL) of DTX or TRQ. **C** Physical stability of CS3 was evaluated by size, PDI, ZP, and EE of DTX and TRQ at $4^\circ C$ for 7 days. Statistical significance was evaluated using Student's *t*-test by comparing the size, PDI, ZP, and EE of 0 days and 7 days. *** $p < 0.001$. Data represent the mean \pm standard deviation ($n = 3$)

High-performance liquid chromatography (HPLC) assay

The amount of DTX, TRQ, DiI, and C6 in samples was quantified using an HPLC (Milford, MA, USA) system consisting of separating modules (Waters® e2695), a UV detector (Waters® e2489), and a data station (Empower® 3). DTX was quantified using a C18 column (Shiseido, 5 µm, 4.6 × 150 mm) with an isocratic mobile phase containing acetonitrile (ACN) and water (55:45, v/v) at a flow rate of 1 mL/min at 25 °C and detected at 230 nm. TRQ was quantified using a C18 column (Kromasil, 5 µm, 4.6 × 150 mm) with a gradient mobile phase containing a mixture of ACN (solvent A) and 0.05% trifluoroacetic acid (solvent B) at a flow rate of 1 mL/min at 30 °C and detected at 254 nm. The following gradient program was applied: 0–8.0 min, 10–80% ACN; 8.0–13.0 min, 80% ACN; 13.0–13.1 min, 80–10% ACN; and 13.1–15.0 min, 10% ACN. DiI was quantified using a C18 column (Shiseido, 5 µm, 4.6 × 150 mm) with an isocratic mobile phase containing 0.05 M dimethyl sulfate and methanol (2:98, v/v) at a flow rate of 1.5 mL/min at 25 °C and detected at 548 nm. C6 was quantified using a C₁₈ column (Kromasil, 5 µm, 4.6 × 150 mm) with an isocratic mobile phase containing ACN and water (4:1, v/v) at a flow rate of 1.5 mL/min at 25 °C and detected at 464 nm. All injection volumes were 50 µL.

Determination of EE and DL

EE and DL of NLC and liposomes

The EE and DL of cargos such as DTX, TRQ, DiI, and C6 in D/NLC, DT/NLC-PR, and T/L-PR were determined indirectly by an ultrafiltration method reported previously (Kim et al. 2023). Free unencapsulated cargo was separated by Amicon® ultracentrifugal devices (100 kDa MWCO; Millipore, Billerica, MA, USA). Briefly, 500 µL of sample was centrifuged for 20 min at 14,000×g at 25 °C. Then, the amount of free unencapsulated cargo in the filtrate was quantified by HPLC as described above. The following equations were used for the calculations:

$$EE(\%) = \frac{W_T - W_F}{W_L} \times 100, \quad (1)$$

$$DL(\mu\text{g}/\text{mg}) = \frac{W_T - W_F}{W_L}, \quad (2)$$

where W_T , W_F , and W_L represent the total amount of cargo added, the amount of free cargo in the filtrate, and the total amount of lipids added, respectively.

EE and DL of CS

The EE and DL of cargos such as DTX, TRQ, DiI and C6 in the CSs were determined directly during the SDGC process (Sánchez-López et al. 2009). Briefly, the total amount of cargo in the samples was quantified by HPLC as described above, before loading on top of 8% sucrose. After SDGC, the amount of encapsulated cargo in the lower layer was quantified and the lower layer solution was freeze-dried as described above. The total amount of lipids added was calculated by the difference in the total amount of freeze-dried lower layer solution and the total amount of cargo and sugar in the lower layer. The following equations were used for the calculations:

$$EE(\%) = \frac{W_{\text{Low}}}{W_{\text{Sample}}} \times 100, \quad (3)$$

$$DL(\mu\text{g}/\text{mg}) = \frac{W_{\text{Low}}}{W_{T1}}, \quad (4)$$

where W_{Low} , W_{Sample} , W_{T1} , and W_{T2} represent the amount of encapsulated cargo in the lower layer after SDGC, the total amount of cargo loaded on top of the 8% sucrose before SDGC, the total amount of freeze-dried lower layer solution, and the total amount of cargos and sugar in the lower layer after SDGC, respectively.

Transmission electron microscopy (TEM) images

The morphologies of D/NLC, T/L-PR, and D/C-T/S-PR were observed using a TEM (Talos L120C; FEI, Czech) at an acceleration voltage of 120 kV. Briefly, nanoparticles were diluted twice with double-distilled water and dropped on a 200-mesh carbon film grid for 1 min, before negative staining with phosphotungstic acid (2%, w/v) for 1 min. Then, the grid was air-dried to evaporate the surface liquid for 24 h at 25 °C and subjected to TEM.

Confocal laser scanning microscope (CLSM) images

To visualize the DiI- and C6- loaded nanoparticles, fluorescence images of D/NLC, T/L-PR, admix of D/NLC and T/L-PR, and D/C-T/S-PR were taken using a CLSM (LSM 700 Meta; Carl Zeiss, Jena, Germany) under 400 × magnification. Briefly, each nanoparticle sample (2 µL) after double dilution with double-distilled water was loaded on the glass slide and dried for 24 h at 25 °C in the dark. Images were obtained using a CLSM with DiI filter (excitation/emission; 549/565 nm) and C6 filter (excitation/emission; 387/470 nm).

In vitro drug release

The in vitro drug release profiles of DT/NLC-PR and D/C-T/S-PR were evaluated using a dialysis bag diffusion method (Kim et al. 2023). Briefly, 1.5 mL of DT/NLC-PR or D/C-T/S-PR with a DTX-equivalent amount of 300 µg were placed in a dialysis bag (100 kDa MWCO; Spectrum Laboratories, Rancho Dominguez, CA, USA). Then, the dialysis bags were soaked in 100 mL of PBS (0.01 M, pH 7.4) containing SDS (1%, w/v) and incubated at 37 °C for 48 h using a magnetic stirrer at 100 rpm. At designated time points, 750 µL of the released medium was collected to analyze the amount of DTX and TRQ and the same volume of fresh release medium was replenished. The amount of DTX and TRQ was analyzed by HPLC as described above.

Cell culture

MCF7 and MCF7/ADR cells were cultured in RPMI 1640 medium containing 10% (v/v) FBS and antibiotics (100 U/mL penicillin G and 100 µg/mL streptomycin). Cells were cultured every 3–4 days in a humidified 5% CO₂ incubator at 37 °C and 95% relative humidity, and cells at passages of 5–20 were used for the experiments.

Cellular uptake

To evaluate the cellular uptake of DTX mediated by RIPL peptide, nanoparticle, and TRQ, DiI was employed to replace DTX. CS-PR, D/C-T/S-P, DT/NLC-PR, and D/C-T/S-PR were evaluated by flow cytometry with CellQuest Pro software (FACSCalibur; Becton Dickinson, Franklin Lakes, NJ, USA) and CLSM images.

For quantitative analysis, MCF7 and MCF7/ADR cells were seeded in 6-well plates at a density of 2×10^5 cells/well and incubated for 24 h at 37 °C. Then, the formulations (DiI-equivalent concentration of 100 ng/mL) were added to the cells and incubated for 90 min at 37 °C. After incubation, the cells were washed twice with PBS, detached by trypsin-EDTA, collected by centrifugation, and resuspended by PBS. Finally, 10,000 cells of each sample were detected by flow cytometry using the FL2 (red) channel.

For qualitative analysis, the same procedure was applied until 90 min incubation in MCF7/ADR cells. After incubation, the cells were washed twice with PBS, fixed with 4% formaldehyde in PBS, and mounted with DAPI to stain nuclei. Finally, fluorescence images of DAPI and DiI were taken using a CLSM under 400× magnification.

Cell viability assay

The cytotoxic effects of D-Sol, admix of D-Sol and T-Sol with a 1:1 mass ratio of DTX and TRQ (D-Sol + T-Sol),

DT/NLC-PR, D/C-T/S-P, and D/C-T/S-PR were evaluated by WST-1 assay using MCF7 and MCF7/ADR cells. On the first day, the cells were seeded into 96-well plates at a density of 1×10^4 cells/well and incubated for 24 h in a humidified 5% CO₂ incubator at 37 °C. On the second day, the cells were treated at 1, 10, 50, 100, 1000, and 10,000 ng/mL as DTX-equivalent concentration and incubated for 24 h. On the third day, cells were washed with PBS and incubated with 100 µL of WST-1 reagent solution (10%, v/v) for 30 min at 37 °C. Finally, the absorbance of each well was measured at 450 nm using a Flexstation 3 microplate reader (Molecular Devices LLC, Sunnyvale, CA, USA). The relative viability of the treated cells was calculated as a percentage of the viability of the untreated control group. Half-maximal inhibitory concentration (IC₅₀) values were determined using GraphPad Prism 7.05 via nonlinear regression. Separately, the cytotoxic effects CS-PR without DTX and TRQ were evaluated by the same procedure except that cells were treated at 0.025, 0.25, 1.25, 2.5, 25, and 250 ng/mL as DiI-equivalent concentration.

Statistical analysis

All data are expressed as the mean ± standard deviation (SD) ($n \geq 3$). Statistical analysis was conducted using the Student's t-test or one-way analysis of variance (ANOVA) followed by Tukey's test for post hoc multiple comparisons. Statistical significance was considered at * $p < 0.05$, ** $p < 0.01$, and *** $p < 0.001$.

Results

Purification and optimization of CS

CSs, D/NLC, and T/L-PR were subjected to SDGC to purify the CS (Fig. 2A). The SDGC process performed at 4 °C prevents spontaneous disruption of nanoparticles by overheating the suspension (Sánchez-López et al. 2009). After SDGC, D/NLC and T/L-PR were not sedimented in the lower layer, but CSs were sedimented and were more frequently observed in the lower layer when the lipid ratio of shell to core was increased.

After sampling the lower layer solution, the physicochemical properties, including the size, PDI, ZP, EE, and DL, of CSs were evaluated to select an optimal ratio (Fig. 2B). One-way ANOVA was used to evaluate the D/NLC and CSs acquired from the lower layer according to size, ZP, EE, and DL (Table S1). The size of all CSs ranged from 190 to 200 nm, with no significant changes in size between CSs. The PDI values of all CSs were < 0.3 , indicating a homogenous particle distribution. The absolute values of ZP and EE of DTX were increased from

CS1 to CS3, with no significant differences thereafter. In contrast, the EE of TRQ increased to approximately 64.1% as the lipid ratio of the shell to core increased. The DL of DTX and TRQ increased from CS1 to CS3, while DTX and TRQ decreased thereafter due to the increase in the total lipid amount. To confirm maintenance of DTX in the core and TRQ in the shell without significant mass transfer between core and shell compartments over time, and to confirm the physical stability of the final formulation, particle size, PDI, ZP, and EE of DTX and TRQ of CS3 were measured at 4 °C after 7 days of preparation (Fig. 2C). Except for the EE of TRQ, no statistically significant changes were found in size, PDI, ZP, and EE of DTX. The EE of DTX measured on the 7th day remained very high EE (97.5%), it was considered that CS3 remained stable and did not significantly affect the stability of the loaded drugs. The slight decrease of EE of TRQ will be due to the fast diffusion of drugs to the release media. Based on these results, CS3 was selected as the D/C-T/S-PR for use in subsequent experiments due to its high EE, DL.

Confirmation of CS formation

As depicted in Fig. 3A, the TEM images showed various spheroid nanoparticles without aggregation. The particle size observed by TEM was consistent with the data acquired from DLS. In particular, a distinct inner core and lipid bilayer outer shell were observed in D/C-T/S-PR.

CSLM images of nanoparticles are shown in Fig. 3B. DiI-loaded D/NLC and C6-loaded T/L-PR showed red and green fluorescence, respectively, while in the admix of these two formulations, red and green fluorescence were observed, respectively, which indicated that each nanoparticle existed separately. In the case of D/C-T/S-PR, orange fluorescence was observed due to the overlay of the DiI-loaded core and C6-loaded shell.

Physicochemical properties of nanoparticles

The physicochemical properties, including the nanoparticle size, PDI, ZP, DL, and EE, of various nanoparticles were evaluated (Table 1). Compared to the size of D/NLC, that of DT/NLC-PR was increased by linkage with DSPE-PEG3K and DSPE-PEG2K-RIPL peptide (Kim et al. 2022). Additionally, compared to the size of D/NLC, that of CSs was increased to approximately 200 nm by the addition of a surface-modified lipid bilayer shell (Wang and Ho 2010). Moreover, there were no significant changes in size between CSs. The PDI values of all formulations were < 0.3, indicating a narrow and homogenous size distribution. In terms of ZP, all types of nanoparticles were negatively charged, but there were differences in the absolute ZP. Compared to the absolute ZP value of D/NLC, those of DT/NLC-PR and T/L-PR were slightly decreased. Among the CSs, the absolute ZP value of D/C-T/S-PR was lower than that of CS-PR without DTX and TRQ and D/C-T/S-P without RIPL peptide. All types of nanoparticles showed a high EE and DL of drug or fluorescent material.

Drug release

The cumulative drug release patterns of DT/NLC-PR and D/C-T/S-PR over 48 h are shown in Fig. 4. In the case of DT/NLC-PR, the release of TRQ and DTX was 66.1% and 73.8% at 6 h, respectively, and reached a plateau after 12 h. Approximately 81% of TRQ and DTX were simultaneously released from the DT/NLC-PR within 12 h. In the case of D/C-T/S-PR, the release of TRQ and DTX was 84.8% and 62.2% at 6 h, respectively, and reached a plateau after 12 h. Approximately 96.7% of TRQ was burst released, while only 71.3% of DTX was released in a more sustained manner from D/C-T/S-PR within 12 h.

Table 1 Physicochemical properties of various nanoparticles

	D/NLC	DT/NLC-PR	T/L-PR	CS-PR	D/C-T/S-P	D/C-T/S-PR
Size (nm)	115.9 ± 3.0	228.5 ± 5.1	121.1 ± 3.1	195.4 ± 2.5	201.4 ± 5.4	202.4 ± 9.6
PDI	0.273 ± 0.048	0.243 ± 0.086	0.139 ± 0.040	0.195 ± 0.072	0.182 ± 0.052	0.225 ± 0.063
ZP (mV)	- 9.8 ± 0.4	- 7.0 ± 0.4	- 7.1 ± 0.5	- 35.2 ± 1.5	- 36.2 ± 2.1	- 32.7 ± 1.4
EE of DTX (%)	99.1 ± 0.1	98.8 ± 0.1	N/A	N/A	45.2 ± 2.5	48.7 ± 3.7
EE of TRQ (%)	N/A	99.8 ± 0.1	40.8 ± 0.1	N/A	44.5 ± 1.4	45.5 ± 0.7
EE of DiI (%)	99.5 ± 0.1	99.6 ± 0.1	N/A	46.5 ± 1.3	45.5 ± 2.1	47.2 ± 1.5
EE of C6 (%)	N/A	N/A	97.5 ± 0.1	45.5 ± 1.1	45.2 ± 1.7	45.6 ± 1.1
DL of DTX (µg/mg)	77.9 ± 1.8	73.3 ± 5.1	N/A	N/A	46.2 ± 2.4	54.4 ± 4.6
DL of TRQ (µg/mg)	N/A	75.8 ± 1.2	77.9 ± 2.0	N/A	47.2 ± 3.1	50.6 ± 4.3

D/NLC docetaxel (DTX)-loaded nanostructured lipid carrier, DT/NLC-PR DTX- and tariquidar (TRQ)-loaded NLC conjugated with PEG and RIPL peptide, T/L-PR TRQ-loaded liposome-PR, CS-PR empty core-shell-PR, D/C-T/S-P DTX-loaded core and TRQ-loaded shell conjugated with PEG, D/C-T/S-PR DTX-loaded core and TRQ-loaded shell-PR, PDI polydispersity index, ZP zeta potential, EE encapsulation efficiency, DL drug loading, N/A not available

The release patterns of D/C-T/S-PR showed a sequential release of TRQ and DTX, whereas those of DT/NLC-PR showed the simultaneous release of TRQ and DTX.

Cellular uptake

The *in vitro* cellular uptake of DiI-loaded formulations, including CS-PR, D/C-T/S-P, DT/NLC-PR, and D/C-T/S-PR, was evaluated in MCF7 and MCF7/ADR cells. DiI was employed to replace DTX to easily quantify and visualize the amount of encapsulated cargo through fluorescence. As shown in Fig. 5A, the mean fluorescence intensity (MFI) values arranged in descending order in MCF7 cells were as follows: D/C-T/S-PR > CS-PR > DT/NLC-PR > D/C-T/S-P. Compared to the MFI values of D/C-T/S-PR in MCF7 cells, those of DT/NLC-PR and D/C-T/S-P were significantly different. Separately, the MFI values arranged in descending order in MCF7/ADR cells were as follows: D/C-T/S-PR > DT/NLC-PR > D/C-T/S-P > CS-PR. Compared to the MFI values of D/C-T/S-PR in MCF7/ADR cells, those of CS-PR, DT/NLC-PR, and D/C-T/S-P were significantly different. As shown in Fig. 5B, the DiI uptake in MCF7/ADR cells following treatment with various formulations was visualized by CLSM. The cells treated with D/C-T/S-PR showed the highest red fluorescence intensity of DiI. The fluorescence intensity of all formulations was consistent with the quantitative analysis results obtained by FACS.

Cytotoxicity

Using the WST-1 assay, we next evaluated the *in vitro* cytotoxicity of D-Sol, D-Sol + T-Sol, D/C-T/S-P, DT/NLC-PR, and D/C-T/S-PR against MCF7 and MCF7/ADR cells at different concentrations of DTX over 24 h (Fig. 5C). The cell viability in the untreated group was considered 100%. In both cell types, concentration-dependent cytotoxicity was observed in all formulations. A gradual decrease in cell viability was observed at concentrations greater than the DTX-equivalent of 10 ng/mL for both cells. When adding T-Sol, the cytotoxicity of D-Sol did not significantly influence DTX cytotoxicity in MCF7 cells; however, the cytotoxicity of D-Sol increased when adding T-Sol to MCF7/ADR cells. In MCF7 cells, there were significant differences in cell viability between concentrations of DT/NLC-PR and D/C-T/S-PR greater than 100 ng/mL of the DTX-equivalent concentration; however, in MCF7/ADR cells, there were significant differences in cell viability between DT/NLC-PR and D/C-T/S-PR at concentrations greater than 10 ng/mL of the DTX-equivalent concentration. Separately, as depicted in Fig. S1, CS-PR without DTX and TRQ resulted in cell viability greater than 95% in all concentrations of DiI.

Table 2 Half-maximal inhibitory concentration (IC₅₀) of different formulations in MCF7 and MCF7/ADR cells

	IC ₅₀ (ng/mL)	
	MCF7	MCF7/ADR
D-Sol	868.9 ± 251.2	7,486.0 ± 274.7
D-Sol + T-Sol	634.9 ± 137.4	2,043.8 ± 631.7
D/C-T/S-P	540.8 ± 70.3	1,203.4 ± 169.2
DT/NLC-PR	164.1 ± 23.8	806.5 ± 90.1
D/C-T/S-PR	99.7 ± 26.2	313.5 ± 99.5

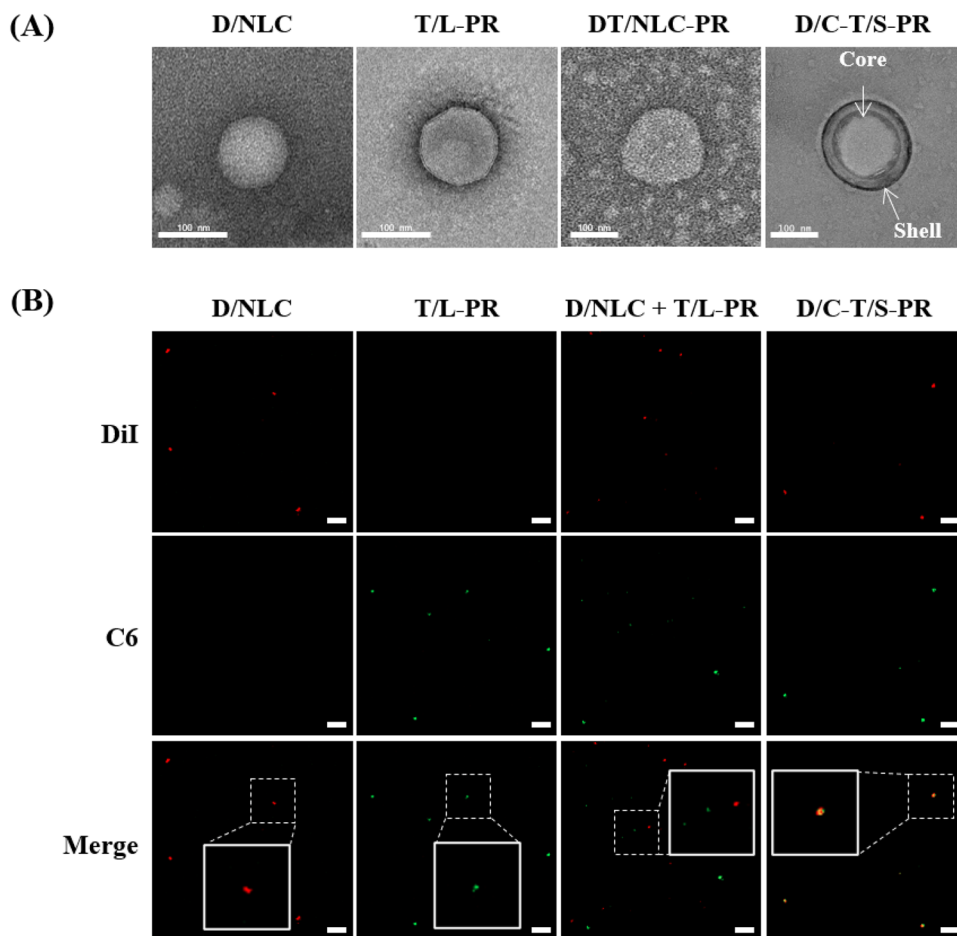
For further comparison, IC₅₀ values were calculated in DTX-loaded formulations (Fig. S2 and Table 2). The IC₅₀ values arranged in ascending order in both cell types were as follows: D/C-T/S-PR < DT/NLC-PR < D/C-T/S-P < D-Sol + T-Sol < D-Sol. MCF7/ADR cells required a higher dose of DTX to achieve an equal level of cell death as that observed in MCF7 cells, which may be due to continuous drug efflux from cells.

Discussion

The D/C-T/S-PR was designed to load drugs into each space for sequential release. The core was composed of D/NLC, while the shell comprised a TRQ-loaded lipid bilayer, which has a long circulation by PEGylation, as well as target modulation by RIPL peptide conjugation (Fig. 1).

The major principle involved in the generation of CS was that the shell consisting of phospholipids became disordered from an ordered state at temperatures higher than the transition temperature and spontaneously wrapped around the core (Mandal et al. 2016). To envelope the core more efficiently, it is important to alter the shell composition and lipid ratio (Troutier et al. 2005). Regarding the shell composition, cholesterol or surfactant can be added to the phospholipids. However, in the case of the addition of cholesterol, the shell did not wrap the core efficiently due to its rigidity (Kalam et al. 2020). In contrast, when surfactant was added to the flexible lipid bilayer shell, it was able to surround the core material more efficiently (Li et al. 2012). The flexibility and permeability of the membrane can be increased by softening the bilayer composition, and a flexible membrane can easily shape and disrupt its membrane (Li et al. 2012). For this reason, Tween 20 was selected as the shell composition. As the lipid ratio of the shell, CSs can be made with different lipid ratios to modulate the amount of lipid that can form the CS and load the maximum amount of drug (Zhang et al. 2008). The lipid density of the shell is also important for steady release of the drug from the core (Wang and Ho 2010).

Fig. 3 Confirmation of core–shell formation. **A** Transmission electron microscopy images of the docetaxel (DTX)-loaded nanostructured lipid carrier (D/NLC), tariquidar (TRQ)-loaded liposome conjugated with PEG and RIPL peptide (T/L-PR), DTX- and TRQ-loaded NLC-PR (DT/NLC-PR), and DTX-loaded core and TRQ-loaded shell-PR (D/C-T/S-PR). Scale bar represents 100 nm. **B** Confocal laser scanning microscopy images of D/NLC, T/L-PR, admix of D/NLC and T/L-PR, and D/C-T/S-PR. Diiodo-3,3',3'-tetramethylindocarbocyanine perchlorate (DiI) and Coumarin 6 (C6) were visualized. Zoom images in a selected dashed line are represented in a box. Scale bar represents 5 μm



Because of these properties, it was necessary to optimize the composition and lipid ratio of the shell.

SDGC was used to purify the CS from the unencapsulated drugs and nanoparticles exist only as core or shell (Fig. 2A). There are several purification methods, including SDGC, ultracentrifugation, and size-exclusion chromatography (Sun et al. 2009; Romana et al. 2020; Pirok et al. 2017). SDGC is based on the principle that specific nanoparticles can be separated at designated sucrose gradients according to separation factors, which are determined by differences in the density, size, and shape of the nanoparticle (Sánchez-López et al. 2009). Sucrose is commonly used given that it forms a discontinuous concentration gradient and is less reactive with other substances (Sánchez-López et al. 2009). In comparison, ultracentrifugation based on size and density generally requires a high gravity force to sediment lipid-based nanoparticles (Romana et al. 2020), while size-exclusion chromatography is only separated by size (Pirok et al. 2017). Considering the separation factors, SDGC was considered the most suitable method to separate the CS. We set a specific sucrose gradient (8%, w/v) where only the CS exists without nanoparticles present as the core or shell. At the

specific sucrose gradient, D/NLC and T/L-PR were not sedimented, whereas CSs were. In particular, more CS nanoparticles were observed as the lipid ratio of the shell increased. After collecting the lower layer of the CSs, the physicochemical properties were evaluated by one-way ANOVA (Fig. S1). As a result, we found no significant differences in the size, ZP and EE of DTX from CS3 to CS5. In the case of DL, CS3 showed the highest DL of DTX and TRQ among all CSs. Finally, CS3 was selected as the D/C-T/S-PR.

As depicted in Table 1, all nanoparticles were < 300 nm, which makes it easier for nanoparticles to cross the enlarged gap junction of cancer cells and accumulate in tumor tissues by the enhanced permeability and retention effect (Fang et al. 2011). Surface modification of NLC and liposomes with PEG and RIPL peptide have been shown to lead to an increase in size (Jang et al. 2019; Kim et al. 2022). However, there were no significant differences in size between D/T-T/S-P and D/T-T/S-PR due to the efficient surface coverage of the PEG chain (Kim et al. 2018). Moreover, when comparing the CS-PR and D/C-T/S-PR, the encapsulation of DTX and TRQ did not appear to affect the size of the CS. Despite the positively charged amine group of TRQ

Fig. 4 In vitro cumulative drug release patterns of docetaxel (DTX) and tariquidar (TRQ) from DTX- and TRQ-loaded nanostructured lipid carrier conjugated with PEG and RIPL peptide (DT/NLC-PR), and DTX-loaded core and TRQ-loaded shell-PR (D/C-T/S-PR) for 48 h. Data represent the mean \pm standard deviation (n=3)

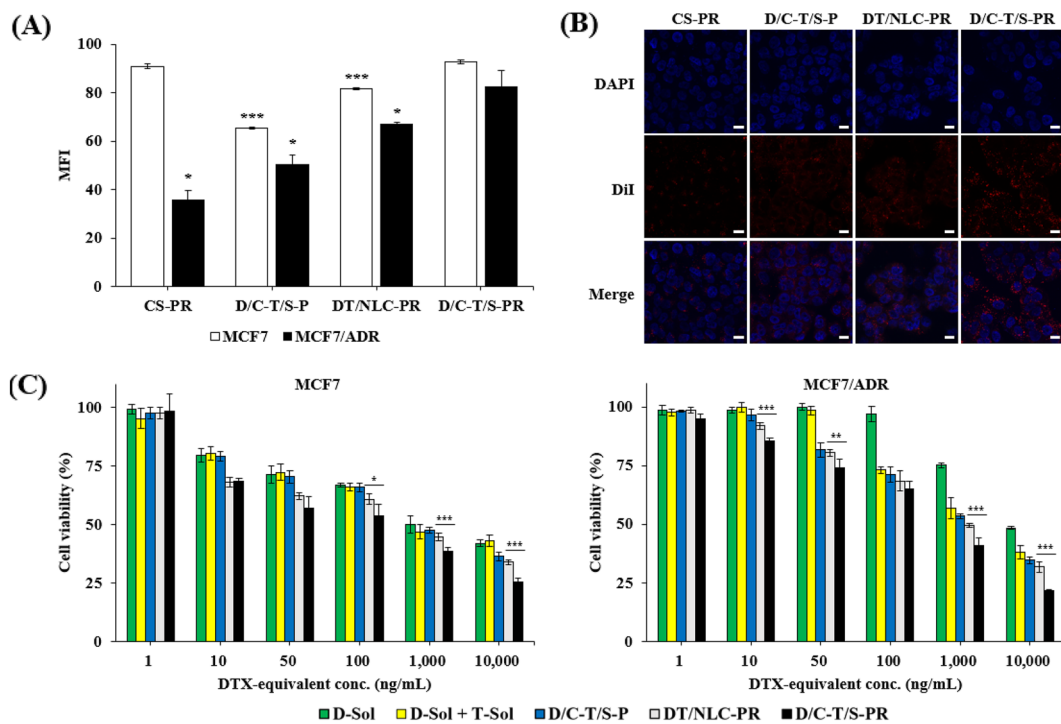
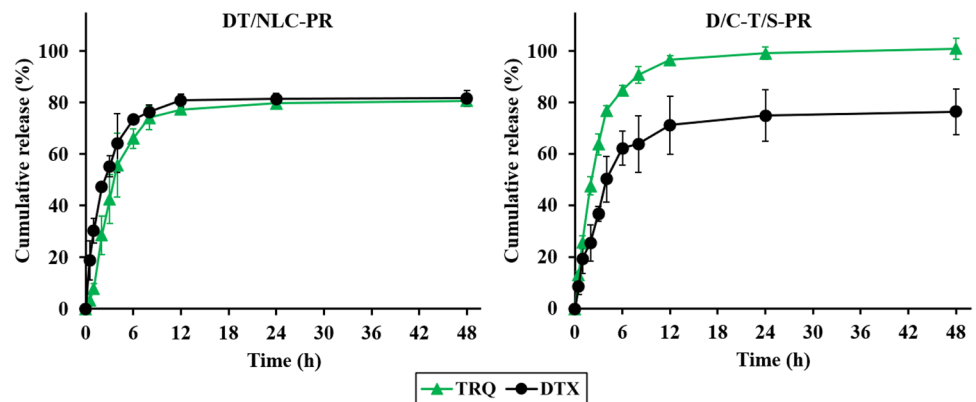


Fig. 5 Cellular uptake and cell viability of various formulations. **A** Mean fluorescence (MFI) values of DiI in core-shell nanoparticles against MCF7 and MCF7/ADR cells after 90 min incubation. Data represent the mean \pm standard deviation (SD) (n=3). Statistical significance was evaluated using the Student's t-test versus docetaxel (DTX)-loaded core and tariquidar (TRQ)-loaded shell conjugated with PEG and RIPL peptide (D/C-T/S-PR). * p < 0.05, ** p < 0.01, and *** p < 0.001. **B** Cellular uptake of core-shell nanoparticles by MCF7/

ADR cells after 90 min incubation. Blue and red represent DAPI and DiI fluorescence, respectively. Scale bar represents 5 μ m. **C** Cell viability of different formulations in MCF7 and MCF7/ADR cells. Data represent the mean \pm SD (n=5). Statistical significance was evaluated using Student's t-test between DTX-loaded and TRQ-loaded nanostructured lipid carrier-PR (DT/NLC-PR) and D/C-T/S-PR. * p < 0.05, ** p < 0.01, and *** p < 0.001

or arginine residue of the RIPL peptide, the ZP value of the T/L-PR or CSs showed a negative charge because the negatively charged PEG chain was sufficient to cover the surface (Kim et al. 2022). The differences in the ZP value between T/L-PR and D/C-T/S-PR were due to the DL differences in TRQ in the lipid bilayer. The absolute ZP value of D/T/S-PR was lower than that of CS-PR or D/C-T/S-P because CS-PR has no TRQ in the shell and D/C-T/S-P has

no RIPL peptide on the surface. In the case of the EE and DL of DTX and TRQ, the NLC formulations showed a high EE of > 98% and a DL of > 73 μ g/mg. Liposomes and CSs showed a relatively low EE and DL, which may be attributed to the spontaneous formation of the lipid membrane, which cannot encapsulate all drugs.

TEM and CLSM images were acquired to confirm the formation of the CS (Fig. 3). In the TEM images, the structure

of the core and shell was observed. Additionally, through the empty space between the core and shell, it could be seen that the shell was composed of a bilayer not a monolayer. In the CLSM images, the overlay of fluorescent images of the DiI-loaded core and C6-loaded shell was observed. These images showed that the 2 fluorescent materials were encapsulated in the core and shell, respectively, and coexisted in the same core-shell structure (Wang and Ho 2010), indicating successful construction of co-loaded CS nanoparticles.

Regarding the release patterns, D/C-T/S-PR showed sequential release of TRQ and DTX, while DT/NLC-PR showed simultaneous drug release (Fig. 4). The CS releases drugs sequentially due to three reasons. First, the core and the shell are structurally positioned inside and outside, respectively, so that the drugs in the outer shell exhibit a burst release pattern unlike those in the inner core. For example, Wang and Ho (2010) generated a CS with a combretastatin-loaded shell and paclitaxel-loaded core and showed 63% burst release of combretastatin and 40% sustained release of paclitaxel in the first 24 h. Additionally, Sengupta et al. (2005) generated a CS where combretastatin loaded to the shell and doxorubicin loaded to the core showed temporal release of combretastatin and doxorubicin. Second, adding surfactant as a component of the lipid bilayer membrane allows rapid release of the drug from the membrane (Kalam et al. 2020). Surfactants such as Tween 20 reduce interfacial tension and increase the permeability of the bilayer, resulting in fast drug release in the lipid bilayer (Cipolla et al. 2014). Third, sustained release patterns of the core can be acquired by optimizing the lipid ratio of the shell (Wang and Ho 2010). At a sufficient lipid ratio of the shell to form a CS, the rate of hydrolysis of the core can be decreased due to the reduced water penetration into the core, which results in slow release of core drugs (Zhang et al. 2008). Therefore, the DTX release pattern from the D/NLC core could be regulated according to the lipid density of the shell.

In the *in vitro* cell study, D/C-T/S-PR exhibited enhanced uptake and cytotoxicity in both cell types. These results are due to the effective internalization by RIPL peptide and nanoparticle, as well as the burst release of TRQ, which sufficiently suppresses the P-gp pump, followed by enhanced accumulation of DTX. Regarding cellular uptake, DiI, a fluorescent material, was used to replace DTX and evaluate the degree of internalization quantitatively and visually. As depicted in Fig. 5A, in the quantitative evaluation by flow cytometry, compared to the MFI value of D/C-T/S-PR, there were no significant differences from that of CS-PR in MCF7 cells, but there were significant differences in MCF7/ADR cells. These findings indicate that P-gp expression was high in MCF7/ADR cells and the P-gp pump was suppressed by TRQ, which can be used for MDR evaluation. In both cell types, the MFI value of D/C-T/S-PR was significantly higher

than that of D/C-T/S-P without RIPL peptide, which showed that RIPL peptide exposure on the surface of the nanoparticle enabled targeting of hepsin-expressing cells and receptor-mediated endocytosis (Kim et al. 2022). Additionally, the MFI value of D/C-T/S-PR was significantly higher than that of DT/NLC-PR in both cell types, which may be attributed to the different cellular internalization capacity of nanoparticles in both cells and the efficient suppression of the P-gp pump by rapidly released TRQ in MCF7/ADR cells.

In the *in vitro* cytotoxicity experiment, CS-PR showed cytotoxicity of > 95% of all DiI concentrations in both cells, indicating that the empty carrier had limited cytotoxicity (Fig. S1). As TRQ is not involved in cytotoxic pathways (Leitner et al. 2011) and shows little to no cytotoxicity (Kim et al. 2022), the cytotoxicity was attributed to DTX. Moreover, when T-Sol was added to D-Sol, the cytotoxicity increased in MCF7/ADR cells, which results from the suppression of the overexpressed P-gp pump by TRQ. Furthermore, D/C-T/S-P showed lower cytotoxicity and higher IC₅₀ values than D/C-T/S-PR in both cell types, indicating that internalization by RIPL peptide is also related to cytotoxicity. Compared to DT/NLC-PR, D/C-T/S-PR showed increased cytotoxicity in both cell types because CS nanoparticles act more efficiently than NLC nanoparticles in both cells. In MCF7/ADR cells, the differences in cytotoxicity between DT/NLC-PR and D/C-T/S-PR may be attributed to effective P-gp blocking of the rapidly released TRQ from the shell, as described in the release data above, followed by continuous accumulation of DTX in the cell (Zhang et al. 2017).

In our previous report, Kim et al. (2022) designed dual carrier system containing DTX-loaded NLC functionalized with PEG and RIPL peptide (DTX-P/R-N) and TQR-loaded NLC functionalized with PEG and RIPL peptide (TRQ-P/R-N). Meanwhile, Kim et al. (2023) reported single carrier system called DT/NLC-PR, which were used as a control group in the current study. In the two reports, co-delivery system showed high EE and high DL capacity at an optimized synergistic mass ratio of DTX:TRQ (1:1). Especially, single carrier system showed more enhanced cytotoxic effect, MDR reversal efficiency, superior cellular uptake, and *in vivo* antitumor efficacy than dual carrier system. Because the present CS system was constructed under the assumption that TRQ located in the shell will be released quickly and inhibit P-gp as a first step, it would have efficiently blocked the P-gp pumps and allowed DTX to be accumulated sufficiently within the cytosols of cells. As depicted in Fig. 6, D/C-T/S-PR is internalized into the cells at higher levels than DT/NLC-PR owing to the different cellular internalization capacities of nanoparticles. After endosomal escape, nanoparticles introduced into the cells without unencapsulated drugs release their drug into the cytoplasm, while TRQ enhances the accumulation of DTX by inhibiting p-gp pump

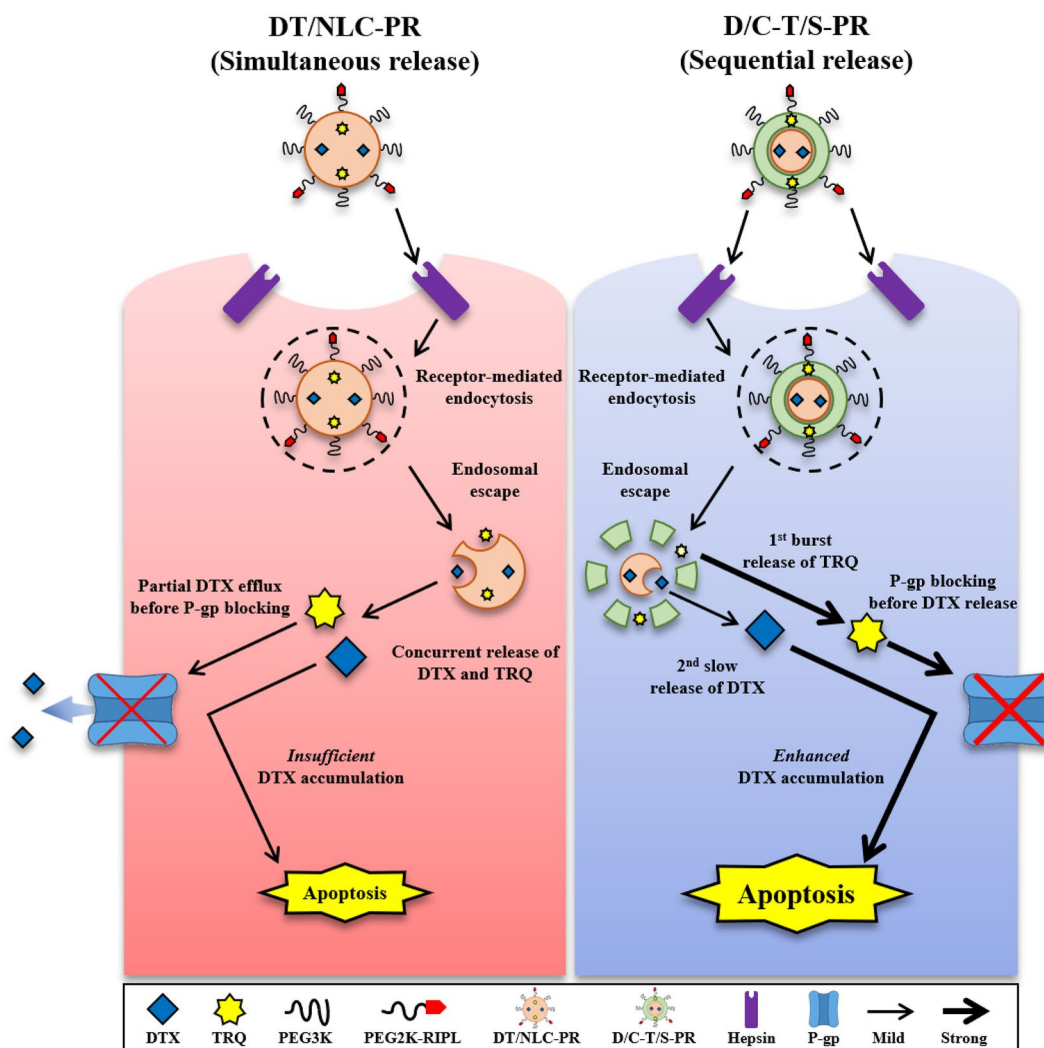


Fig. 6 Comparison of the antitumor efficacy between docetaxel (DTX)- and tariquidar (TRQ)-loaded nanostructured lipid carrier conjugated with PEG and RIPL peptide (DT/NLC-PR), and DTX-loaded core and TRQ-loaded shell-PR (D/C-T/S-PR). RIPL peptide can bind to overexpressed hepsin receptor, which induces internalization by receptor-mediated endocytosis. D/C-T/S-PR showed enhanced internalization compared to DT/NLC-PR. DT/NLC-PR escapes from

efflux (Yu et al. 2020). Moreover, DTX induces microtubule stabilization, G2/M phase arrest, and finally apoptotic cell death (Herbst and Khuri 2003). At this time, in the case of DT/NLC-PR, partial DTX efflux occurs before P-gp blocking of TRQ; however, in the case of D/C-T/S-PR, P-gp is blocked by the rapid release of TRQ followed by sustained release of DTX. Then, high concentrations of DTX from the CS could be accumulated due to the inhibition of DTX efflux, which further enhances the effect of apoptosis. Therefore, improved internalization at specific ligand-receptor interaction and rapid P-gp inhibition by P-gp inhibitor can induce enhanced antitumor activity in MDR cancer (Zhang et al. 2017; Lee and Lee 2023).

the endosomes and simultaneously releases TRQ and DTX into the cytosol (left panel). In comparison, D/C-T/S-PR escapes from the endosomes and sequentially releases TRQ and DTX into the cytosol (right panel). Compared to DT/NLC-PR, rapidly released TRQ from D/C-T/S-PR may inhibit the P-glycoprotein (P-gp) before DTX efflux and enhance DTX accumulation, which enhances apoptosis.

Conclusion

Here, we successfully developed D/C-T/S-PR for the sequential release of TRQ and DTX. CSs with diverse lipid ratios of the shell were evaluated to acquire CSs with a high EE, DL, and sequential release. As the lipid ratio of the shell to core increases, relatively more CSs were sedimented after SDGC and CS3 was selected as the final formulation, with homogenous dispersion (202.4 nm), ZP (−32.7 mv), EE of DTX (48.7%), EE of TRQ (45.5%), DL of DTX (54.4 μg/mg), and DL of TRQ (50.6 μg/mg). Through the TEM images, the distinct core and shell from D/C-T/S-PR were observed with no aggregation. In the CLSM images, the

coexistence of fluorescent materials in the core and shell was confirmed by observing the overlay of fluorescence images of the DiI-loaded core and C6-loaded shell. In terms of the drug release patterns, D/C-T/S-PR initially showed a burst release pattern of TRQ and subsequently showed a sustained release pattern of DTX.

Regarding cellular uptake, D/C-T/S-PR showed enhanced nanoparticle internalization capacity. In terms of cell viability, D/C-T/S-PR showed high cytotoxicity and a low IC₅₀ value in both cell types tested. Therefore, the sequential delivery of TRQ and DTX using D/C-T/S-PR represents a good candidate to overcome MDR. However, further studies on in vitro and in vivo experiments are still needed.

Supplementary Information The online version contains supplementary material available at <https://doi.org/10.1007/s40005-023-00645-8>.

Acknowledgements This study was funded by the National Research Foundation of Korea (NRF) grant funded by the Korea government (MSIT) (No. 2022R1A2B5B02001794). This research was supported by CAU GPF Program through the Chung-Ang University in 2023 funded by BrainKorea21 Four. We also thank Prof. Dr. Kyung Hoon Min (College of Pharmacy, Chung-Ang University, Seoul, Korea) for kindly providing the MCF7/ADR cells for this study.

Declarations

Conflict of interest All authors (H.M. Jung, C.H. Kim, J.E. Seo, Y.T. Goo, S.H. Hong, M.J. Kang, S. Lee, and Y.W. Choi) declare that they have no conflicts of interest.

Research involving human and animal participation This article does not contain any studies on human or animal subjects performed by any of the authors.

References

- Cipolla D, Wu H, Gonda I, Eastman S, Redelmeier T et al (2014) Modifying the release properties of liposomes toward personalized medicine. *J Pharm Sci* 103:1851–1862
- Fang J, Nakamura H, Maeda H (2011) The EPR effect: unique features of tumor blood vessels for drug delivery, factors involved, and limitations and augmentation of the effect. *Adv Drug Deliv Rev* 63:136–151
- Guo Y, He W, Yang S, Zhao D, Li Z et al (2017) Co-delivery of docetaxel and verapamil by reduction-sensitive PEG-PLGA-SS-DTX conjugate micelles to reverse the multi-drug resistance of breast cancer. *Colloids Surf B* 151:119–127
- Herbst RS, Khuri FR (2003) Mode of action of docetaxel—a basis for combination with novel anticancer agents. *Cancer Treat Rev* 29:407–415
- Jang MH, Kim CH, Yoon HY, Sung SW, Goh MS et al (2019) Steric stabilization of RIPL peptide-conjugated liposomes and in vitro assessment. *J Pharm Investig* 49:115–125
- Jiang L, Lee HW, Loo SCJ (2020) Therapeutic lipid-coated hybrid nanoparticles against bacterial infections. *RSC Adv* 10:8497–8517
- Kalam MA, Alkholief M, Badran M, Alshememry A, Alshamsan A (2020) Co-encapsulation of metformin hydrochloride and reserpine into flexible liposomes: characterization and comparison of in vitro release profile. *J Drug Deliv Sci Technol* 57:101670
- Kang MH, Park MJ, Yoo HJ, Lee SG, Kim SR, Yeom DW, Kang MJ, Choi YW (2014) RIPL peptide (IPLVVPLRRRRRRRC)-conjugated liposomes for enhanced intracellular drug delivery to hepsin-expressing cancer cells. *Eur J Pharm Biopharm* 87:489–499
- Kim CH, Sung SW, Lee ES, Kang TH, Yoon HY et al (2018) Sterically stabilized RIPL peptide-conjugated nanostructured lipid carriers: characterization, cellular uptake, cytotoxicity, and biodistribution. *Pharmaceutics* 10:199
- Kim CH, Lee TH, Kim BD, Kim HK, Lyu MJ et al (2022) Co-administration of tariquidar using functionalized nanostructured lipid carriers overcomes resistance to docetaxel in multidrug resistant MCF7/ADR cells. *J Drug Deliv Sci Technol* 71:103323
- Kim CH, Lee S, Choi JY, Lyu MJ, Jung HM et al (2023) Functionalized lipid nanocarriers for simultaneous delivery of docetaxel and tariquidar to chemoresistant cancer cells. *Pharmaceutics* 16:349
- Lee E, Lee ES (2023) Tumor extracellular vesicles carrying antitumor (KLAKLAK) 2 peptide and tumor-specific antigens for improved tumor therapy. *J Pharm Investig* 53:505–516
- Lee J, Kim J, Kang J, Lee HJ (2023) COVID-19 drugs: potential interaction with ATP-binding cassette transporters P-glycoprotein and breast cancer resistance protein. *J Pharm Investig* 53:191–212
- Leitner I, Nemeth J, Feurstein T, Abraham A, Matzneller P et al (2011) The third-generation P-glycoprotein inhibitor tariquidar may overcome bacterial multidrug resistance by increasing intracellular drug concentration. *J Antimicrob Chemother* 66:834–839
- Li C, Zhang Y, Su T, Feng L, Long Y et al (2012) Silica-coated flexible liposomes as a nanohybrid delivery system for enhanced oral bioavailability of curcumin. *Int J Nanomed* 7:5995–6002
- Li N, Mai Y, Liu Q, Gou G, Yang J (2021) Docetaxel-loaded D- α -tocopheryl polyethylene glycol-1000 succinate liposomes improve Lung cancer chemotherapy and reverse multidrug resistance. *Drug Deliv Transl* 11:131–141
- Mandal B, Bhattacharjee H, Mittal N, Sah H, Balabathula P et al (2013) Core-shell-type lipid-polymer hybrid nanoparticles as a drug delivery platform. *Nanomedicine: NBM* 9:474–491
- Mandal B, Mittal NK, Balabathula P, Thoma LA, Wood GC (2016) Development and in vitro evaluation of core-shell type lipid-polymer hybrid nanoparticles for the delivery of erlotinib in non-small cell Lung cancer. *Eur J Pharm Sci* 81:162–171
- Patel K, Chowdhury N, Doddapaneni R, Boakye CH, Godugu C et al (2015) Piperlongumine for enhancing oral bioavailability and cytotoxicity of docetaxel in triple-negative breast cancer. *J Pharm Sci* 104:4417–4426
- Patil Y, Sadhukha T, Ma L, Panyam J (2009) Nanoparticle-mediated simultaneous and targeted delivery of paclitaxel and tariquidar overcomes tumor drug resistance. *J Control Rel* 136:21–29
- Pirok BW, Breuer P, Hoppe SJ, Chitty M, Welch E et al (2017) Size-exclusion chromatography using core-shell particles. *J Chromatogr A* 1486:96–102
- Romana B, Hassan MM, Sonvico F, Pereira GG, Mason AF et al (2020) A liposome-micelle-hybrid (LMH) oral delivery system for poorly water-soluble drugs: enhancing solubilisation and intestinal transport. *Eur J Pharm Biopharm* 154:338–347
- Ruttala HB, Ko YT (2015) Liposomal co-delivery of curcumin and albumin/paclitaxel nanoparticle for enhanced synergistic antitumor efficacy. *Colloids Surf B* 128:419–426
- Sánchez-López V, Fernandez-Romero J, Gómez-Hens A (2009) Evaluation of liposome populations using a sucrose density gradient centrifugation approach coupled to a continuous flow system. *Anal Chim Acta* 645:79–85
- Sarisozen C, Vural I, Levchenko T, Hincal AA, Torchilin VP (2012) Long-circulating PEG-PE micelles co-loaded with paclitaxel and elacridar (GG918) overcome multidrug resistance. *Drug Deliv* 19:363–370

- Sengupta S, Eavarone D, Capila I, Zhao G, Watson N et al (2005) Temporal targeting of tumour cells and neovasculature with a nanoscale delivery system. *Nature* 436:568–572
- Sun X, Tabakman SM, Seo WS, Zhang L, Zhang G et al (2009) Separation of nanoparticles in a density gradient: FeCo@C and gold nanocrystals. *Angew Chem* 121:957–960
- Thapa RK, Kim JO (2023) Nanomedicine-based commercial formulations: current developments and future prospects. *J Pharm Investig* 53:19–33
- Thomas H, Coley HM (2003) Overcoming multidrug resistance in cancer: an update on the clinical strategy of inhibiting p-glycoprotein. *Cancer Control* 10:159–165
- Troutier A-L, Delair T, Pichot C, Ladavière C (2005) Physicochemical and interfacial investigation of lipid/polymer particle assemblies. *Langmuir* 21:1305–1313
- Wang Z, Ho PC (2010) Self-assembled core-shell vascular-targeted nanocapsules for temporal antivasculature and anticancer activities. *Small* 6:2576–2583
- Xia Y, Fang M, Dong J, Xu C, Liao Z et al (2018) pH sensitive liposomes delivering tariquidar and doxorubicin to overcome multidrug resistance of resistant ovarian cancer cells. *Colloids Surf B* 170:514–520
- Xu C, Ding Y, Ni J, Yin L, Zhou J et al (2016) Tumor-targeted docetaxel-loaded hyaluronic acid-quercetin polymeric micelles with p-gp inhibitory property for hepatic cancer therapy. *RSC Adv* 6:27542–27556
- Yap TA, Omlin A, De Bono JS (2013) Development of therapeutic combinations targeting major cancer signaling pathways. *J Clin Oncol* 31:1592–1605
- Yin Y-M, Cui F-D, Mu C-F, Choi M-K, Kim JS et al (2009) Docetaxel microemulsion for enhanced oral bioavailability: preparation and in vitro and in vivo evaluation. *J Control Rel* 140:86–94
- Yu J, Hu F, Zhu Q, Li X, Ren H et al (2020) PD-L1 monoclonal antibody-decorated nanoliposomes loaded with paclitaxel and P-gp transport inhibitor for the synergistic chemotherapy against multidrug resistant gastric cancers. *Nanoscale Res Lett* 15:1–13
- Zhang L, Chan JM, Gu FX, Rhee J-W, Wang AZ et al (2008) Self-assembled lipid-polymer hybrid nanoparticles: a robust drug delivery platform. *ACS Nano* 2:1696–1702
- Zhang J, Wang L, Fai Chan H, Xie W, Chen S et al (2017) Co-delivery of paclitaxel and tetrandrine via iRGD peptide conjugated lipid-polymer hybrid nanoparticles overcome multidrug resistance in cancer cells. *Sci Rep* 7:46057
- Zhong P, Chen X, Guo R, Chen X, Chen Z et al (2020) Folic acid-modified nanoerythrocyte for codelivery of paclitaxel and tariquidar to overcome breast cancer multidrug resistance. *Mol Pharm* 17:1114–1126

Publisher's Note Springer Nature remains neutral with regard to jurisdictional claims in published maps and institutional affiliations.

Springer Nature or its licensor (e.g. a society or other partner) holds exclusive rights to this article under a publishing agreement with the author(s) or other rightsholder(s); author self-archiving of the accepted manuscript version of this article is solely governed by the terms of such publishing agreement and applicable law.

Authors and Affiliations

Hyun Min Jung¹ · Chang Hyun Kim^{1,2} · Jo-Eun Seo¹ · Yoon Tae Goo¹ · Sun Ho Hong¹ · Myung Joo Kang³ · Sangkil Lee¹ · Young Wook Choi¹

✉ Sangkil Lee
skdavid@cau.ac.kr

✉ Young Wook Choi
ywchoi@cau.ac.kr

Hyun Min Jung
hmin1229@naver.com

Chang Hyun Kim
yj.ch.kim@gmail.com

Jo-Eun Seo
jo Eun0405@hanmail.net

Yoon Tae Goo
rndbsxo5318@naver.com

Sun Ho Hong
bcbf2326@naver.com

Myung Joo Kang
kangmj@dankook.ac.kr

¹ College of Pharmacy, Chung-Ang University, 84 Heukseok-ro, Dongjak-gu, Seoul 06974, Republic of Korea

² Department of Pharmaceutical Sciences, University of North Texas Health Science Center, Fort Worth, TX 76107, USA

³ College of Pharmacy, Dankook University, 119 Dandae-ro, Dongnam-gu, Cheonan, Chungnam 31116, Republic of Korea